Cell Biol Toxicol (2021) 37:193–207
https://doi.org/10.1007/s10565-020-09528-2

ORIGINAL ARTICLE

Cytoplasmic sirtuin 6 translocation mediated by p62 polyubiquitination plays a critical role in cadmium-induced kidney toxicity

Keum-Young So · Byung-Hyun Park · Seon-Hee Oh

Received: 15 January 2020 / Accepted: 15 April 2020 / Published online: 11 May 2020

Abstract Sirtuin 6 (Sirt6) is important for maintaining kidney homeostasis and function. Cd exposure increases the risk of developing kidney diseases. However, the role of Sirt6 in kidney disease mechanisms is unclear. Here, we evaluated the role of Sirt6 in Cd-induced kidney toxicity. After Cd exposure, p62/sequestosome-1 (SQSTM1), an autophagy substrate, accumulated in mouse kidney mesangial cells in monomeric and polyubiquitinated (polyUb) forms. Sirt6 accumulated in response to Cd treatment at concentrations below the half-maximal inhibitory concentration and decreased after 12 h of treatment. Sirt6 and p62 co-localized in the nucleus and redistributed to the cytosol after Cd treatment. Sirt6 was mainly present in nuclei-rich membrane fractions. Sirt6 interacted with p62. Ub, and microtubule-associated protein light chain 3 (LC3). Knockdown of p62 promoted Sirt6 nuclear accumulation and inhibited apoptosis. Sirt6 overexpression altered levels of polyUb-p62 and apoptosis. At earlier times during Cd treatment, polyubiquitination of p62 and apoptosis were reduced. Cytoplasmic translocation of Sirt6 occurred later, with increased polyubiquitination of p62 and apoptosis. Bafilomycin 1 (BaF1) treatment promoted cytosolic Sirt6 accumulation, increasing cell death. Silencing *autophagy related 5* (*Atg5*) increased nuclear Sirt6 levels, reduced polyUb-p62, and inhibited cell death, indicating that autophagy was necessary for Sirt6 redistribution. Cd resistance was associated with reduced polyUb-p62 and persistent Sirt6 expression. Cd treatment in mice for 4 weeks promoted p62, Sirt6, and LC3-II accumulation, inducing apoptosis in kidney tissues. Overall, our findings show that polyUb-p62 targeted Sirt6 to autophagosomes, playing a crucial role in Cd-induced cell death and kidney damage.

Keywords Autophagy · Cadmium · Mesangial cells · p62 · Polyubiquitination · Sirt6

Electronic supplementary material The online version of this article (https://doi.org/10.1007/s10565-020-09528-2) contains supplementary material, which is available to authorized users.

K.-Y. So
Department of Anesthesiology and Pain Medicine, School of Medicine, Chosun University, 309 Pilmundaero, Dong-gu, Gwangju 501-759, South Korea

B.-H. Park
Department of Biochemistry, Chonbuk National University Medical School, Jeonju, Jeonbuk, Republic of Korea

S.-H. Oh (✉)
School of Medicine, Chosun University, 309 Pilmundaero, Dong-gu, Gwangju 501-759, South Korea
e-mail: seonh@chosun.ac.kr

Introduction

The kidneys are essential for maintaining homeostasis in the body by filtering blood and removing waste as urine (Guyton 1991). These vital organs are damaged by various stressors that affect their function that can result in severe diseases. A number of acute and chronic insults, including those caused by drugs, toxins, metabolism, and inflammation, can damage the kidneys

(Kimura et al. 2017; Lee et al. 2018; Satarug and Moore 2004). Humans are continuously exposed to Cd, a toxic heavy metal, from contaminated foods, industrial sources, and cigarette smoke (Järup 2003). Cd accumulates in various tissues and organs; however, the kidney is very sensitive to Cd exposure (Johri et al. 2010). Cd-induced kidney toxicity has been extensively studied at the molecular level. Apoptosis is triggered by various signaling pathways, including endoplasmic reticulum stress, and plays a critical role in kidney injury (Fujiwara et al. 2012; Kitamura and Hiramatsu 2010). In mammals, sirtuin proteins (Sirt1–7) are NAD^+-dependent deacetylases and ADP ribosylases. Sirtuins are involved in multiple signaling pathways related to aging, DNA repair, inflammation, and metabolic diseases, such as diabetes and cancer (Wang et al. 2019). Sirtuins also play critical roles in kidney diseases (Kitada et al. 2013; Morigi et al. 2018). Sirt1, the most extensively studied sirtuin, is associated with regulating blood pressure by decreasing epithelial sodium reabsorption in collecting duct cells. Sirt1 also protects kidneys against ischemia/reperfusion, cisplatin-induced acute kidney injury, and renal fibrosis (Fan et al. 2013; Hasegawa et al. 2010; He et al. 2010; Zhang et al. 2009). Sirt3 localizes to mitochondria, along with Sirt4 and Sirt5, and is a key regulator of mitochondrial redox status by modulating superoxide dismutase 2 (SOD2) acetylation. Sirt3 downregulation leads to tubular injury and renal dysfunction (Ouyang et al. 2019; Yu et al. 2012). Recent studies have shown Sirt6 involvement in kidney diseases (Liu et al. 2017). Sirt6 deficiencies in mice induce podocyte injury, kidney hypertrophy, and fibrosis. Sirt6 is downregulated in renal biopsies from patients with podocytopathies. Moreover, Sirt6 protects podocytes against apoptosis, which plays an important role in podocyte homeostasis (Huang et al. 2017). Cd exposure increases the risk of developing renal diseases, where continuous exposure to environmental Cd can be a critical factor in developing chronic kidney disease (Johri et al. 2010; Trzcinka-Ochocka et al. 2004; Wu et al. 2016). Despite the known roles of Sirt6 in kidney diseases, its role in Cd-induced kidney toxicity remains unclear.

Autophagy helps maintain cellular health by inducing lysosomal degradation of proteins and damaged organelles. Autophagy is induced in response to various stresses, such as starvation (Kroemer et al. 2010), and plays an essential role in cell survival against metabolic stresses and immunological responses (Liang and Jung 2010). In contrast, hyper-active autophagy signaling can result in severe pathogenic conditions caused by excessive cell death (Levine and Yuan 2005). Many studies have shown that autophagy is associated with Cd-induced kidney damage; however, this is still controversial. Cd-induced autophagy is associated with kidney damage in mouse and mesangial cells (Luo et al. 2016; Wang et al. 2009). In contrast, autophagy is protective against Cd-induced apoptotic and necrotic cell death in rat kidney mesangial cells and proximal tubular cells (Chargui et al. 2011; Fujishiro et al. 2018; Luo et al. 2017; Wang et al. 2009). Previously, we found that autophagy is protective against Cd-induced apoptosis in NRK52E rat kidney epithelial cells (So and Oh 2016), suggesting that Cd-induced autophagy may be species-specific. Since autophagy can be involved in both cell death and cell survival depending on stress conditions, further studies are needed to clarify functions of autophagy under pathophysiological conditions.

In this study, we aimed to elucidate the role of Sirt6 in Cd-induced kidney damage and the underlying molecular mechanisms related to autophagy. We found that apoptosis induced by Cd was regulated by Sirt6, and that nuclear Sirt6 was targeted by p62/sequestosome-1 (SQSTM1) (referred to as p62) to autophagosomes. Additionally, Sirt6 accumulation in the cytosol played a critical role in Cd-induced apoptosis. These results were confirmed in Cd-resistant cells and mouse kidneys. Collectively, our results suggested that cytosolic Sirt6 may be a biomarker for Cd-induced kidney toxicity, and that polyubiquitinated (polyUb)-p62/Sirt6 signaling may be a potential therapeutic target in Cd-induced kidney damage.

Materials and methods

Reagents and antibodies

Cadmium acetate (289159), bafilomycin A1 (B1793), MG132 (M8699), Hoechst 33342 (B2261), MTT [3-(4,5-dimethylthiazol-2-yl)-2,5-diphenyltetrazolium bromide], and anti-β-actin antibody (ab-8226) were obtained from Sigma-Aldrich. Ubiquitin (sc-8017), p21 (sc-6246), FITC-conjugated goat anti-mouse (sc-2010), and rhodamine-conjugated goat anti-rabbit (sc-2091) antibodies were purchased from Santa Cruz. LC3B (2775, 3868), Sirt6 (12486), PARP-1 (9532), procaspase-3 (9662), cleaved caspase-3 (9661),

caspase-8 (4790), cleaved caspase-8 (9749), NBR1 (9891), phospho-p53 (S15, 9284), CHOP (2895), and phospho-γ-H2AX (S139, 2577) antibodies were purchased from Cell Signaling. SQSTM1/p62 (H00008878-M01) and APG3L (AP1807a) antibodies were purchased from Abnova and Abgent, respectively. HDAC1 (GTX-100513) antibody was purchased from GenTex.

Cell culture

Mouse kidney mesangial MES13E cells were purchased from the American Type Culture Collection (CRL-1927™) and kept in Dulbecco's modified Eagle's medium (WelGene, LM-001-05), supplemented with 10% fetal bovine serum (WelGene, S001-01) and penicillin-streptomycin (Sigma-Aldrich, P4333). The cells were cultured at 37 °C humidified incubator with 5% CO_2. Cells were stored at − 80 °C by using cryopreservation solutions (Revive Organtech, 10002-01). Cells between passage 3~12 were used for all experiments.

Cytotoxicity assays

Cell viability was analyzed by an MTT assay (Sigma, M2128). One hundred fifty microliters of cell suspensions (1×10^5 cells/mL) per well were seeded in a 48-well plate and kept overnight. After chemical treatment, MTT (0.5 mg/mL) was added and continuously kept for 2 h at 37 °C. The absorbance of formazan crystals dissolved in dimethyl sulfoxide was read with a microplate reader (Perkin-Elmer) at 540 nm. Experiments were repeated more than three times. Values were revealed mean ± standard deviation (SD) of fold increase compared with the control.

RNA interference and overexpression

Target-specific siRNAs for Atg5 (5′-GAGUCAGC UAUUUGACGUU-3′) and p62 (5′-CUU GUA GUU GCA UCA CGU A-3′) were synthesized by Bioneer (Daejeon, South Korea). Mouse Sirt6 siRNA (no. 50721) was purchased from Bioneer. Cells were seeded into 6-well plates and performed transfection with 20 pM siRNA or scrambled siRNA (Thermo Fisher Scientific, AM4635) using Lipofectamine™ RNAiMAX reagent (Invitrogen, 56,531). pcDNA3.1-Sirt6 was kindly provided by Dr. Park Byung-Hyun (Chonbuk National Univ.). Plasmid DNA (0.5 μg) and empty vector were transfected into cells using X-tremeGENE DNA transfection kit (Roche, 06366244001) according to the supplier's protocol. Media was replaced with fresh, complete media after 6 h. Cells were incubated for an additional 1–2 days before further treatment.

Subcellular fractionation

Cells were harvested and resuspended in hypotonic solution [20 mM HEPES (pH 7.0), 10 mM KCl, 1 mM sodium- EDTA, 1 mM EGTA, 1.5 mM $MgCl_2$, 0.25 M sucrose (Sigma-Aldrich, S0389)] supplemented with protease inhibitor mixture (Roche Applied Science, 11836170001). The cells were homogenized by passing them through a needle, and then centrifuged at 800×*g* for 4 min at 4 °C. The pellet was the nuclei-rich insoluble fraction. The supernatant was then centrifuged at 10,000×*g* for 20 min at 4 °C. The new supernatant and cytoplasmic organelle-rich pellet were used as the soluble and particulate fractions, respectively.

Immunoblotting and immunoprecipitation

Cells were lysed in lysis buffer (Cell Signaling, 9803) supplemented with protease inhibitors. Proteins (15–35 μg) were resolved by 10–12% SDS-PAGE, and transferred to polyvinylidene difluoride (PVDF) membrane (Millipore, IPVH00010), and blocked with 5% skim milk (Bioshop, SK1400.500). Membranes were probed with each primary antibodies and secondary antibodies. Proteins were detected using a chemiluminescent substrate (Millipore, WBKLS0100). For immunoprecipitation (IP) analysis, total proteins were extracted using lysis buffer [0.05 M Tris-HCl (pH 7.4), 0.25% Triton X-100, 250 mM NaCl, 10% glycerol] with protease inhibitors. Proteins (600 μg) were precleared with 50% protein G Plus-agarose beads (Santa Cruz, sc-2002) and centrifuged at 12,000×*g* for 10 min at 4 °C. The supernatant was reacted with indicated primary antibody or mouse IgG (Sigma-Aldrich, 12-371) or rabbit IgG (Sigma-Aldrich, 12-370) overnight at 4 °C on a rocker. The antibody complexes were captured on protein G Plus-agarose beads and analyzed by western blotting. Protein levels were quantified using Image J software.

Immunofluorescence

Cells were cultured on a cover slip (Marienfeld, D111580) and fixed in 10% neutral-buffered formalin

(Sigma-Aldrich, HT501128) for 12 min on ice, washed with PBS several times, and treated with 0.05% Triton X-100 (Sigma, T8787) for 20 min. Cells were washed with PBS and treated with bovine serum albumin (2%, Bioshop, ALB001.100). The cells were incubated with primary antibodies and fluorescent- tagged secondary antibodies. Nuclei were stained with Hoechst 33342 (1 μg/mL) and captured by using a fluorescence microscope (Nikon Eclipse TE300).

Immunohistochemistry

Tissues were fixed in normal-buffered formalin and embedded in paraffin. Sections (4-μm-thick) were subjected to antigen retrieval in 0.01 M sodium citrate buffer (pH 6). After removing endogenous peroxidase activity using 0.3% H_2O_2, sections were incubated with Sirt6 antibody (Thermo Scientific, PA5-13225, 1:50) overnight at 4 °C. A negative control was performed for each specimen without using the primary antibody. The Polink-2 AP broad detection kit (GBI Labs, D68-18) was used according to the manufacturer's protocol. After counter-staining with hematoxylin, sections were mounted with Simpo-mount (GBI Labs, E01-18).

Animal experiments and Cd treatment

Animal care and Cd treatments were performed as previously described (Kim et al. 2015). Briefly, 6-week-old male C57BL/6 (C57) mice (Orientbio, Seongnam, South Korea) kept under routine conditions with 12 h light-dark cycles at 50–60% humidity. Animal groups were randomly divided into two groups of 8 mice. Mice were treated with cadmium acetate (1 mg/kg body weight) or equivalent saline by i.p. for 4 weeks. The animals were then anesthetized with 5% isoflurane in oxygen. The animal studies were processed after permission from the Institutional Animal Care and Use Committee (IACUC) at Chosun University (approval no.CIACUC2019-A0045).

Statistical analysis

All experiments were performed independently three or more times. Data were presented as mean ± SD. The statistical significance of the differences between the experimental groups was determined by one-way ANOVA with a post hoc test. P values < 0.05 were considered statistically significant.

Results

Cd exposure in MES13 cells

The sensitivity of mouse kidney epithelial cells (SV40-modified MES13) to Cd was analyzed by MTT assay after Cd exposure for 24 h (Fig. 1a). The half-maximal inhibitory concentration (IC_{50}) of Cd is approximately 24 μM. MES13E cells exposed to Cd exhibited morphological features for apoptosis, including rounding or floating into the medium (Fig. 1b). To determine whether Cd sensitivity was associated with apoptosis in MES13 cells, we first investigated expression of apoptotic pathway proteins. Caspase-8, caspase-3, and poly-ADP ribose polymerase 1 (PARP-1) cleavage as well as C/EBP homologous protein (CHOP) induction occurred in a concentration-dependent manner. Consistently, Cd exposure induced phosphorylation of gamma H2A family member X (phospho-γH_2AX, S139), a marker for double-strand DNA breaks, phosphorylation of p53 (S15), and p21 (Fig. 1c), suggesting that Cd caused DNA damage–induced apoptosis. These data indicated that Cd-induced cytotoxicity in MES13 cells was caused by apoptosis through caspase- and endoplasmic reticulum stress-mediated signaling pathways.

Cd-induced autophagy promoted selective accumulation of monomeric and polyUb-p62

Previous studies have shown that autophagy is critical for kidney function (Chargui et al. 2011; Fujishiro et al. 2018; Luo et al. 2017; Wang et al. 2009). We observed autophagy induction through microtubule-associated protein light chain 3 (LC3) conversion by immunoblotting in Cd-exposed MES13 cells. LC3-phosphatidylethanolamine (LC3-II), an autophagy marker, was induced even at low Cd concentrations but did not cause morphological changes related to apoptosis. Despite increased LC3-II expression, monomeric p62 and multiple bands of high molecular weight proteins were detected in a dose-dependent manner. Treatment of cells with Cd at the IC_{50} concentration showed that LC3-II was induced as early as 1 h after treatment. Levels of monomeric and high molecular weight forms of p62 gradually increased over time, and were highest at 24 h (Fig. 2a, b). However, when the membrane was exposed for a longer period of time, a few bands were observed that were below 55 kDa, with a single band detected that was less than 25 kDa (Suppl.

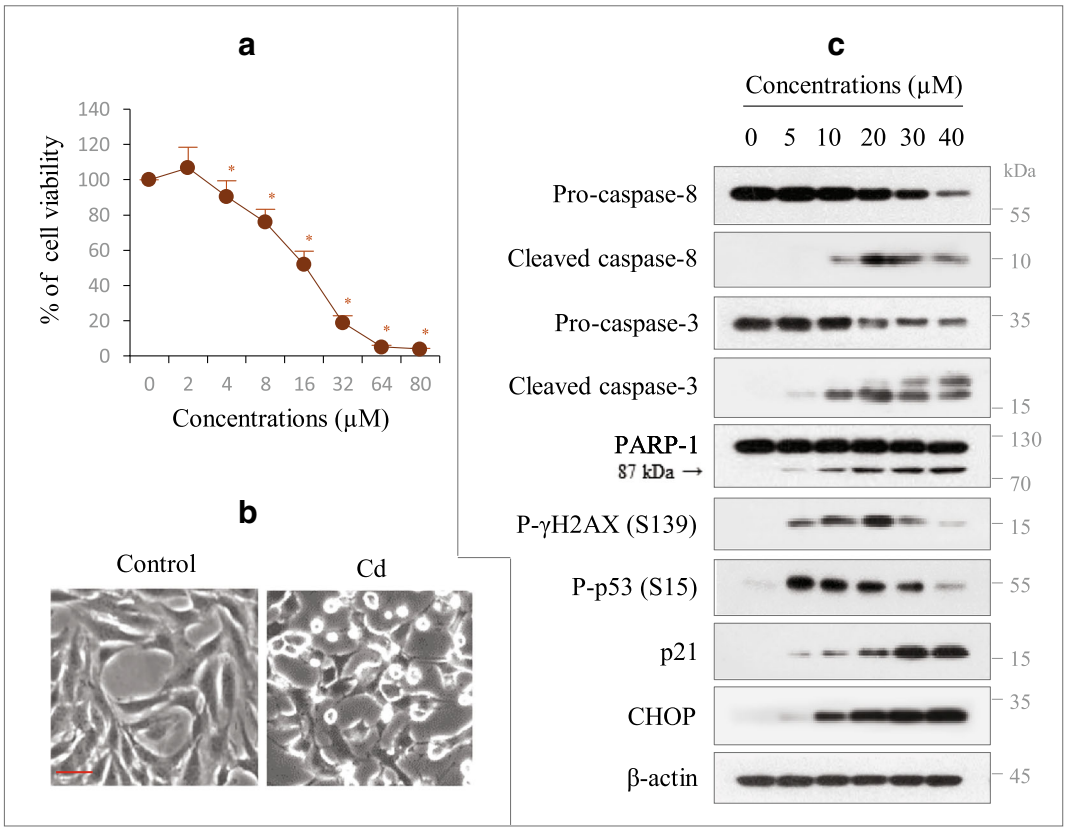

Fig. 1 Effects of Cd on autophagy- and apoptosis-related proteins in MES13 cells. **a** Viability was tested in cells treated with increasing Cd concentrations for 18 h using MTT assay. Data are expressed as mean ± SD of fold increase compared with untreated control from three independent experiments performed in triplicate. **b** Cells were observed by phase-contrast microscopy after 18 h of treatment with 24 μM Cd. Scale bar = 25 μm. **c** Cells were treated as described in **a**. Immunoblotting was performed for indicated proteins. β-Actin was used as the loading control. Cd-treated cells were compared with control cells. $n = 3$. $^*P < 0.05$

Fig. S1). This suggested that Cd could impair p62-mediated autophagy or result in low autophagic flux. However, another selective autophagy substrate, a neighbor of BRCA1 gene 1 (NBR1) (Kirkin et al. 2009), was degraded in a dose- and time-dependent manner (Fig. 2a). Because LC3-II accumulation can be caused by reduced autophagic flux or activation, we examined autophagic flux using bafilomycin A1 (BaF1), an inhibitor of autophagosomal and lysosomal fusion. Pretreatment with BaF1 before Cd exposure for 12 h upregulated LC3-II compared with that in Cd-treated cells without BaF1 pretreatment. Moreover, BaF1 pretreatment slightly increased, but not significantly, monomeric p62 and high molecular weight p62 levels, suggesting that Cd impaired p62-mediated selective autophagic degradation (Fig. 2c, d). These results were further confirmed by silencing *autophagy related 5* (*Atg5*). Cells were transiently transfected with *Atg5*-specific and nonspecific control (NC) small-interfering RNAs (siRNAs). Knockdown (KD) was analyzed by immunoblotting for Atg5 protein 24 h after transfection (Fig. 2e). Atg5 KD inhibited autophagy, demonstrated by decreased LC3-II levels. This modification reduced monomeric p62 and high molecular weight p62 without alteration of the polyUb-protein, indicating that autophagy may be associated with accumulation of high molecular weight p62 (Fig. 2f, g). IP analysis of ubiquitin (Ub) and p62 confirmed that the high molecular weight p62 was polyUb-p62 (Suppl. Fig. S2). Collectively, these findings demonstrated that Cd exposure in MES13 cells could selectively impair p62-mediated autophagy.

p62 co-localized with Sirt6 and regulated its subcellular localization

Sirt6 is important for podocyte homeostasis and maintenance of glomerular function (Huang et al. 2017). To

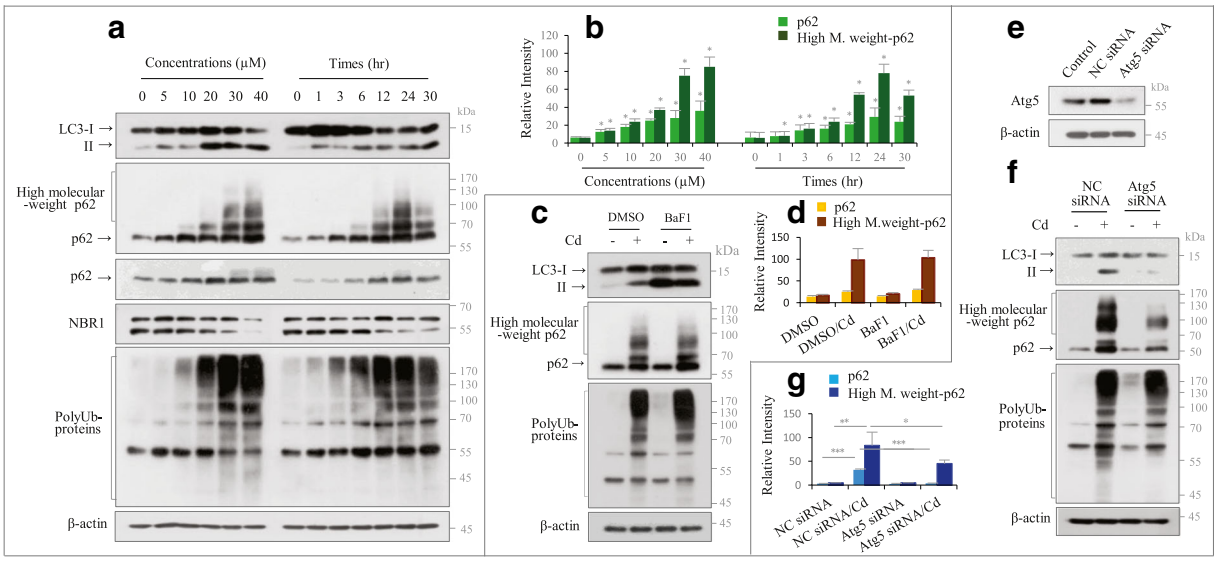

Fig. 2 Cd-induced accumulation of polyUb-p62 was regulated by autophagy. **a**, **b** MES13 cells were treated with increasing Cd concentrations for 18 h or with 24 μM for up to 30 h. Lysates were analyzed by immunoblotting for the indicated proteins. PolyUb-p62 levels were quantified by densitometry and normalized to β-actin. Data are represented as mean ± SD ($n = 3$). *$P < 0.05$. **c**, **d** Cells were exposed to 24 μM Cd for 12 h with or without pretreatment with 20 nM BaF1 for 2 h. p62 levels determined by immunoblotting were normalized to β-actin. **e** After 24 h, knockdown (KD) efficiency using *Atg5*-specific siRNA was evaluated by immunoblotting for Atg5. NC negative control. **f**, **g** Cells transfected with NC and ATG5 siRNA were exposed to 24 μM Cd for 12 h. p62 levels determined by immunoblotting were normalized to β-actin. *$P < 0.05$; **$P < 0.005$; ***$P < 0.0005$

investigate whether Sirt6 was involved in Cd-induced cytotoxicity, Sirt6 protein levels were analyzed in Cd-exposed MES13 cells by immunoblotting. Sirt6 was upregulated in cells treated with Cd at concentrations lower than the IC_{50} compared with that in untreated control cells. Additionally, Sirt6 levels remained high until 6 h, and then gradually decreased in cells treated with Cd at IC_{50} concentration (Fig. 3a, b). We next examined how nuclear Sirt6 was degraded after Cd exposure. We examined the involvement of p62 in Sirt6 degradation because p62 shuttles between the nucleus and cytosol, acting as a cargo receptor for ubiquitinated targets for autophagic or proteasomal degradation (Ichimura et al. 2008; Pankiv et al. 2010). To elucidate interactions between p62 and Sirt6, we performed immunofluorescence (IF) with anti-p62 and anti-Sirt6 antibodies. In untreated control cells, Sirt6 staining was faint and was diffusely distributed in the nucleus. Sirt6 nuclear staining intensity peaked at 3 h after Cd exposure, and then gradually redistributed to the perinuclear area. After 6 h, Sirt6 staining was punctate along the periphery of the nuclear membrane. These structures gradually increased in size and fluorescence intensity. Finally, Sirt6 aggregated in the cytosol after 12 h. Similar kinetics were detected for p62. In untreated control cells, p62 localized mainly to the nucleus, with weak, diffuse distribution in the cytoplasm. After 1 h of Cd exposure, p62 staining was punctate and distributed in the periphery of the nuclear membrane. Increased fluorescence intensity was observed after 3 h, and some cells still showed nuclear distribution. After 6 h, p62 puncta size was increased and localized distinctly in the perinuclear region. Eventually, excessive p62 aggregation in the cytoplasm resulted in a concave nuclear shape and increased condensed chromatin (Fig. 3c). Furthermore, p62 and Sirt6 localization completely overlapped, suggesting the proteins may interact. Subcellular redistribution of p62 and Sirt6 after Cd exposure was further confirmed by subcellular fractionation into insoluble (i.e., nuclei-rich membranes), particulate (i.e., autophagosomes and mitochondria), and soluble (i.e., cytosol) fractions. The purities of the isolated fractions were validated by immunoblotting for specific protein markers, such as histone deacetylase 1 (HDAC1), SOD2, LC3-II, and β-actin for nuclear, mitochondria, autophagosomal, and cytosolic compartments, respectively. In untreated cells, monomeric p62 was present at similar levels in insoluble and soluble fractions, but at

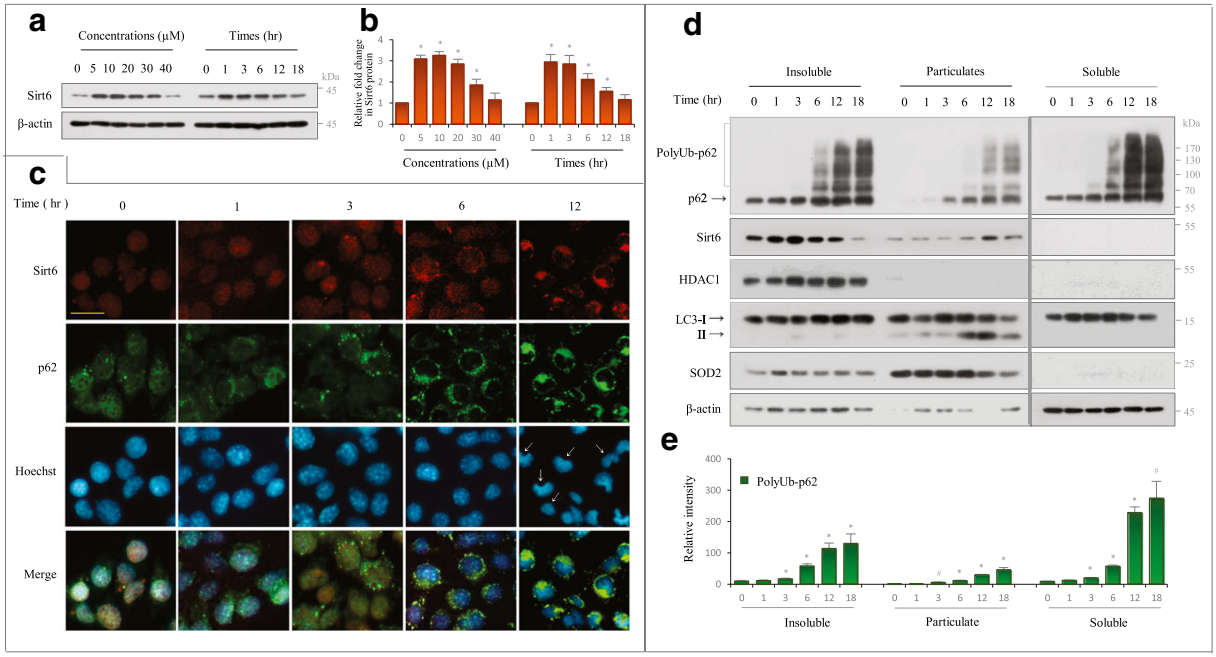

Fig. 3 Subcellular localization of p62 and Sirt6 in Cd-treated MES13 cells. **a** Cells were treated with increasing Cd concentrations for 18 h or with 24 μM Cd (IC_{50}) for up to 18 h. Immunoblotting was performed for Sirt6. β-Actin was used as the loading control. **b** Cells cultured on coverslips were treated with 24 μM Cd, fixed, and then incubated with p62 (green) and Sirt6 (red) antibodies, and subsequently with FITC- and rhodamine-conjugated secondary antibodies, respectively. Nuclei were counterstained with Hoechst 33342 (blue) and images were acquired with a fluorescence microscope. Arrows indicate apoptotic nuclei. Scale bar, 25 μm. **c**, **d** Cells were treated with 24 μM Cd for up to 18 h and subjected to subcellular fractionation into insoluble, particulate, and soluble fractions. The purity of the fractions was determined by immunoblotting for HDAC1, LC3-II, SOD2, and β-actin for nuclear, autophagosomal, mitochondrial, and soluble fractions, respectively. PolyUb-p62 levels were normalized to β-actin. $n = 3$. $^{*}P < 0.05$; $^{\#}P < 0.001$

lower levels in the particulate fractions. After Cd exposure, the levels of p62 and polyUb-p62 increased over time in all three fractions, with the highest amount observed in the soluble fractions. PolyUb-p62 level in the particulate fraction increased at 12 h compared with those in the insoluble and soluble fractions, in which the polyUb-p62 level increased after 6 h. Sirt6 was mainly detected in the insoluble fractions, and redistributed into particulate fractions after 6 h (Fig. 3d, e). Additionally, Sirt6 was not detected in the soluble fractions. These findings indicated that Sirt6 translocated into some organelles, such as autophagosomes. LC3-I was distributed in all three fractions, but LC3-II was detected only in the particulate fraction, indicating that autophagosomes were present in the particulate fractions (Fig. 3d). Thus, p62 and Sirt6 may interact in autophagosomes. We next examined whether Sirt6 translocated with p62 using an inhibitor of nuclear export, leptomycin B (LMB). LMB treatment resulted in increased polyUb-p62 in the insoluble fractions, and decreased polyUb-p62 in the particulate fractions. However, Sirt6 was not increased in insoluble fractions but was decreased in the particulate fractions (Suppl. Fig. S3). These results suggested that subcellular redistribution of Sirt6 may depend on polyUb-p62.

Effects of p62 KD on Cd-induced Sirt6 protein expression and its subcellular distribution

IF staining and fractionation studies for p62 and Sirt6 showed possible interactions between both proteins. Thus, we next examined the role of p62 relative to Sirt6 in Cd-treated MES13 cells using p62-specific siRNA. KD efficiency was analyzed by immunoblotting 24 h after transfection (Fig. 4a). After 12 h of Cd treatment, monomeric p62 and polyUb-p62 decreased in KD cells along with increased Sirt6 and decreased caspase 3-dependent PARP-1 cleavage compared with those in NC siRNA-transfected cells, which had unaffected LC3-II expression and polyUb-p62 levels (Fig. 4b, c).

Next, we examined changes in Sirt6 levels by fractionation analyses. p62 KD decreased monomeric p62

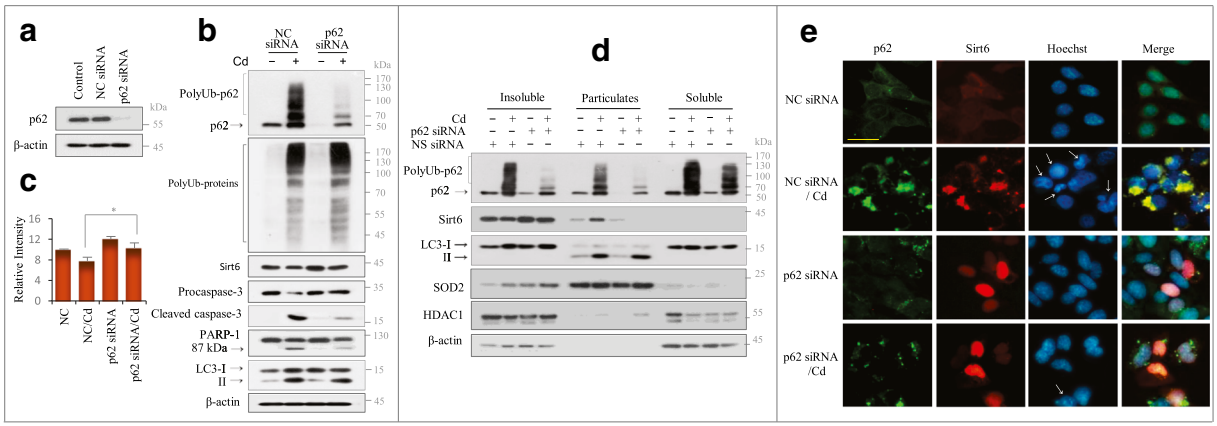

Fig. 4 Effects of p62 KD on Sirt6 and apoptosis. **a** KD in cells transfected with *p62*-specific siRNA was evaluated after 24 h by immunoblotting for p62 protein. NC negative control. **b**, **c** Cells transfected with NC and p62 siRNAs were treated with 24 μM Cd for 12 h. Immunoblotting was performed for indicated proteins. Sirt6 levels were normalized to β-actin. $*P < 0.05$. **d** Cells were treated as described in B and subjected to subcellular fractionation into insoluble, particulate, and soluble fractions. The purity the fractions was determined by immunoblotting for HDAC1, LC3-II/ SOD2, and β-actin for nuclear, particulate, and soluble fractions, respectively. Data are representative of $n > 3$. **e** Cells cultured on coverslips were transfected with p62 siRNA and treated with Cd for 12 h prior to fixation. Cells were then incubated with p62 (green) and Sirt6 (red) antibodies, and subsequently with FITC- and rhodamine-conjugated secondary antibodies. Nuclei were counterstained with Hoechst 33342 (blue) and imaged. Arrows indicate apoptotic nuclei. Scale bar = 25 μm

and polyUb-p62 in all three fractions, particularly in the insoluble and particulate fractions, compared with those in NC siRNA-transfected cells. As expected, p62 KD increased Sirt6 levels in the insoluble fraction, and decreased Sirt6 in the particulate fraction, indicating that p62 regulated subcellular Sirt6 redistribution. The purity of the fractions was confirmed by immunoblotting for specific protein markers, such as HDAC1, SOD2, LC3-II, and β-actin for nuclei, mitochondria, autophagosomes, and cytosol, respectively (Fig. 4c). These results were further verified by IF for p62 and Sirt6. Cd treatment of NC siRNA-transfected cells resulted in p62 and Sirt6 aggregation in the cytoplasm, revealing apoptotic nuclear changes (arrows). p62-KD cells increased Sirt6 in the nucleus compared with NC siRNA-transfected cells, showing diffuse distribution. Cd exposure in p62-KD cells decreased the number of cells with apoptotic features in the nucleus (Fig. 4d). Therefore, these data indicated that p62 may target Sirt6 to the cytosol which results in apoptosis.

Effects of ectopic overexpression and Sirt6 KD on Cd-induced apoptosis

To elucidate the roles of nuclear and cytosolic Sirt6 in Cd-treated MES13 cells, cells were transfected with empty vector and pcDNA3.1-Sirt6. Overexpression of Sirt6 was determined by immunoblotting (Fig. 5a). After transfection, cells were treated with Cd for 12 h, and then IF was performed. In Sirt6-overexpressing cells without Cd treatment, Sirt6 was predominantly localized to the nucleus. In contrast, after Cd treatment, Sirt6 was distributed in both the nucleus and cytoplasm (Fig. 5b, Suppl. Fig. S4a). The results of Sirt6 overexpression were then analyzed by immunoblotting. Cd exposure for 12 h in Sirt6-overexpressing cells slightly reduced Cd-induced monomeric- and polyUb-p62 expression but did not affect other polyUb-proteins (Fig. 5c, d). Additionally, Cd-induced caspase-3 and PARP-1 cleavage slightly decreased (Fig. 5e). However, long Cd exposure (24 h) increased polyUb-p62 levels in the cytosol, where most cells showed severely altered nuclear shapes associated with increased procaspase-3, PARP-1 cleavage, and LC3-II levels (Suppl. Fig. S4b, c). Furthermore, after 8 h Cd treatment, prior to Sirt6 translocation, polyubiquitination of p62 and PARP-1 cleavage was inhibited (Suppl. Fig. S4d). Thus, Sirt6 overexpression appears to induce apoptosis later than wild-type cells, at least during the time it stays in the nucleus. The degree of apoptosis increased with ectopic Sirt6 translocation into the cytoplasm.

Next, we examined the effects of Sirt6 deficiency on Cd-induced cytotoxicity. Immunoblotting was performed in cells transfected with Sirt6-specific and NC siRNAs (Fig. 5f). Cd exposure for 8 h, prior to Sirt6 downregulation, resulted in decreased Cd-induced monomeric and polyUb-p62, and inhibited PARP-1 and

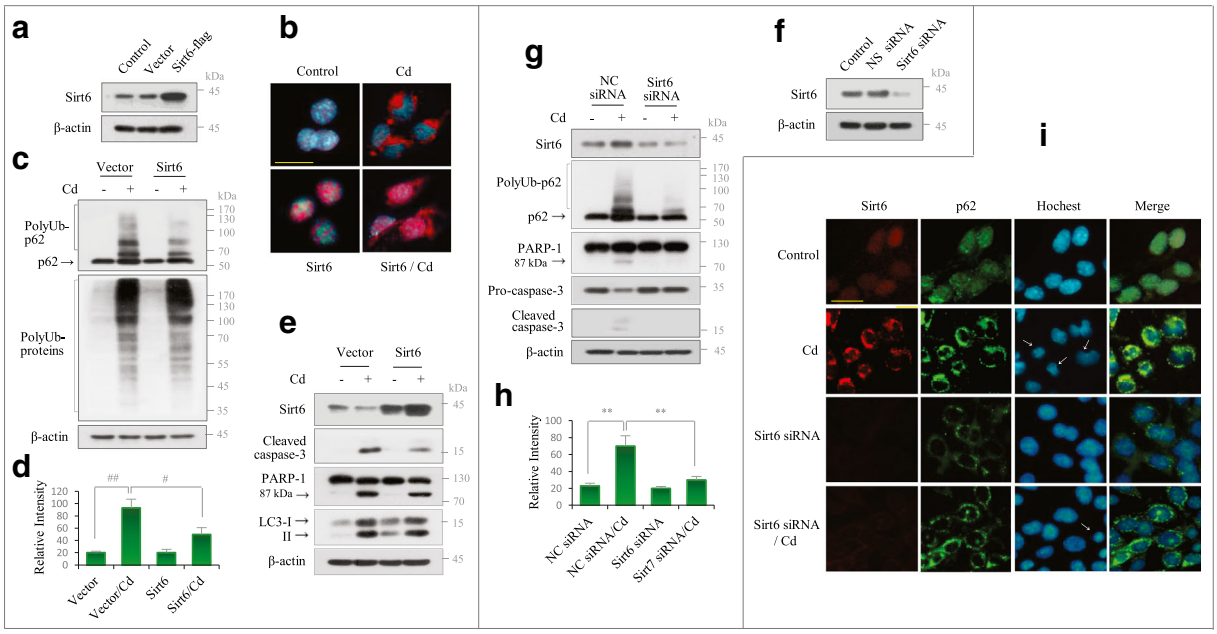

Fig. 5 Effects of Sirt6 subcellular localization on Cd-induced apoptosis. **a** After 24 h of transfection with empty vector and pcDNA3.1-Sirt6, immunoblotting was performed for Sirt6 protein. **b** Cells overexpressing Sirt6 were treated with Cd for 12 h. Cells were fixed and incubated with Sirt6 antibody and rhodamine-conjugated secondary antibody. Nuclei were counterstained with Hoechst 33342. Scale bar = 25 μm. **c**–**e** Cells overexpressing Sirt6 were treated with 24 μM for 12 h. Immunoblotting was performed for indicated proteins. PolyUb-p62 levels were normalized to β-actin. $^{\#}P < 0.01$, $^{\#\#}P < 0.0001$. **f** After 24 h of transfection with NC- and *Sirt6*-specific siRNAs, immunoblotting was performed for Sirt6 protein. β-Actin was used as the loading control. **g**, **h** Sirt6-KD cells were exposed to 24 μM Cd for 8 h. Immunoblotting was performed for indicated proteins. β-actin was used as the loading control. PolyUb-p62 levels were normalized to β-actin. $^{*}P < 0.005$. **i** Cells transfected with Sirt6 siRNA were treated with Cd for 12 h. Cells were fixed and incubated with p62 (green) and Sirt6 (red) antibodies. Nuclei were counterstained with Hoechst 33342 (blue) and imaged. Arrows, apoptotic nuclei. Scale bar = 25 μm

procaspase-3 cleavage (Fig. 5g, h). The results were confirmed by IF for Sirt6 and p62. Sirt6 deficiency reduced p62 punctate structures and inhibited Cd-induced nuclear apoptotic changes (Fig. 5i). Collectively, these results indicated that Sirt6 redistribution into the cytosol was regulated by p62, and may be involved in Cd-induced apoptosis.

Sirt6 interacted with Ub via p62 in Cd-treated MES13 cells

In this study, we found that p62 was polyubiquitinated and co-localized with Sirt6 in response to Cd. To elucidate whether the interactions between these proteins were related to Ub, IP assay for Ub was performed in lysates from cells treated with Cd for 6 h and 12 h, followed by immunoblotting with an anti-Sirt6 antibody (Fig. 6a, b). Inversely, IP analysis for Sirt6 and rabbit IgG was performed with the same protein lysates, followed by immunoblotting with an anti-Ub antibody (Fig. 6c, d). These results indicated that Sirt6 interacted with Ub.

Next, we examined the direct interaction between p62 and Sirt6. IP was performed in lysates from cells treated with Cd for 6 h and 12 h with Sirt6 and rabbit IgG antibodies, followed by immunoblotting with anti-p62 antibody (Fig. 6e, f). Furthermore, IP was performed in lysates of Sirt6-overexpressing cells with anti-p62 antibody, followed by immunoblotting with anti-Sirt6 antibody (Fig. 6g, h). From these experiments, we found that p62 interacted with Sirt6. However, our results showed that Sirt6 may indirectly interact with Ub via p62. To clarify this, we performed IP assays for Sirt6 with lysates from p62-KD cells, followed by immunoblotting with anti-Ub antibody, and vice versa. p62 KD significantly inhibited the interaction between Ub and Sirt6 (Fig. 6i–l), indicating that Sirt6 indirectly interacted with Ub via p62.

PolyUb-p62 targeted Sirt6 to autophagosomes

In the above experiments, we found that p62 interacted with Sirt6 through IP and IF assays. Additionally, Sirt6 protein levels gradually decreased after 6 h of Cd

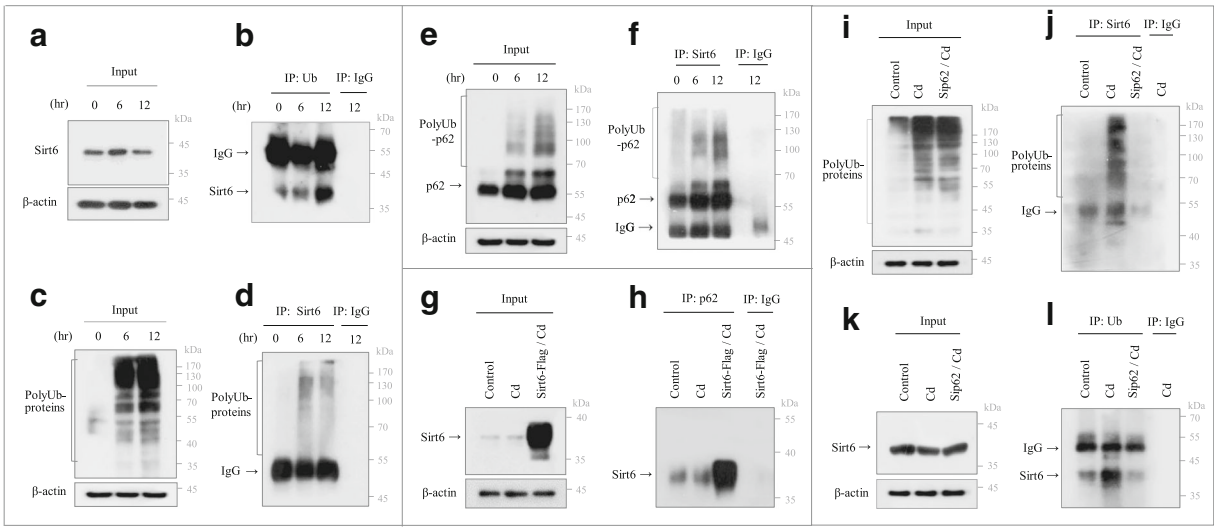

Fig. 6 Sirt6 interacted with Ub via p62. **a**, **b** Cells were treated with 24 μM Cd for 6 h or 12 h. Immunoblotting was performed for Sirt6 (input), where immunoprecipitation (IP) was performed with 600 μg of the remaining protein with Ub antibody, followed by immunoblotting for Sirt6 or (**c**, **d**) vice versa. **e**, **f** Cells were treated with 24 μM Cd for 6 h or 12 h. Immunoblotting was performed for p62 (input), where IP was performed with 600 μg of the remaining protein with Sirt6 antibody, followed by immunoblotting for p62. **g**, **h** Cells overexpressing Sirt6 were treated with Cd for 12 h. Immunoblotting was performed for Sirt6 (input), where IP was performed with 600 μg of the remaining protein with p62 antibody, followed by immunoblotting for Sirt6. **i**–**l** p62-KD cells were treated with 24 μM Cd for 12 h, and immunoblotting was performed with **i** Ub or **k** Sirt6 antibodies. IP was performed with 600 μg of the remaining protein with **j** Sirt6 or **l** Ub antibodies, followed by immunoblotting for Ub or Sirt6, respectively. $n > 3$

exposure (Fig. 3a). Therefore, we questioned whether p62 could target Sirt6 to autophagosomes or to proteasomes for degradation. We examined whether Sirt6 was regulated by lysosomal degradation using BaF1. We confirmed that BaF1 treatment before Cd exposure induced LC3-II accumulation, indicating that BaF1 inhibited autophagic degradation (Fig. 2c). BaF1 pretreatment enhanced procaspase-3 and PARP-1 cleavage (Fig. 7a) and increased Sirt6 levels compared with those in Cd-treated cells. These findings were confirmed by IF for p62 and Sirt6. BaF1 treatment further enhanced Cd-induced p62 and Sirt6 aggregation in the cytosol (Suppl. Fig. S5), showing that inhibition of autophagic flux could block Sirt6 degradation. These results were further confirmed by silencing *Atg5*. Suppression of autophagy by *Atg5* KD was confirmed (Fig. 2e, f). We also observed partial inhibition of caspase-3-mediated PARP-1 cleavage, and upregulation of Cd-induced Sirt6 levels (Fig. 7b). Inhibition of autophagosome degradation by BaF1 treatment or inhibition of autophagosome formation by *Atg5* KD resulted in increased Sirt6 protein levels; however, cell viability was inconsistent. Therefore, we examined cellular distribution of Sirt6 during *Atg5* KD by IF. Sirt6 and p62 were evenly distributed in the nucleus in *Atg5*-KD cells. Moreover, in Cd-treated *Atg5*-KD cells, Sirt6 was prominently distributed in the nucleus and periphery of the nuclear membrane. p62 accumulated in a small number of large punctate structures in the periphery of the nuclear membrane (Fig. 7c). Consistent with these findings, nuclear accumulation of Sirt6 was confirmed by fractionation studies (Suppl. Fig. S6), indicating that deficient autophagy inhibited Sirt6 translocation into the cytosol, disrupting aggregation of p62 and Sirt6 proteins.

Next, to examine whether Sirt6 and p62 interacted with LC3, IP assays were performed for LC3B and rabbit IgG in lysates from Cd-exposed MES13 cells. Immunoblotting was performed for p62 and Sirt6. LC3B immunocomplexes interacted with polyUb-p62 (Fig. 7d, e) and Sirt6 (Fig. 7f, g), demonstrating that polyUb-p62 and Sirt6 were recruited into autophagosomes. We also examined the involvement of proteasomes in Sirt6 degradation. Inhibition of proteasomes by MG132 treatment (0.25–1 μM) increased Cd-induced polyubiquitination of p62 and other proteins, but did not upregulate Sirt6 and LC3-II levels (Suppl. Fig. S7). This showed that Sirt6 levels were not dependent on the proteasome degradation pathway. These findings suggested that autophagy played a critical role in regulating Sirt6 levels.

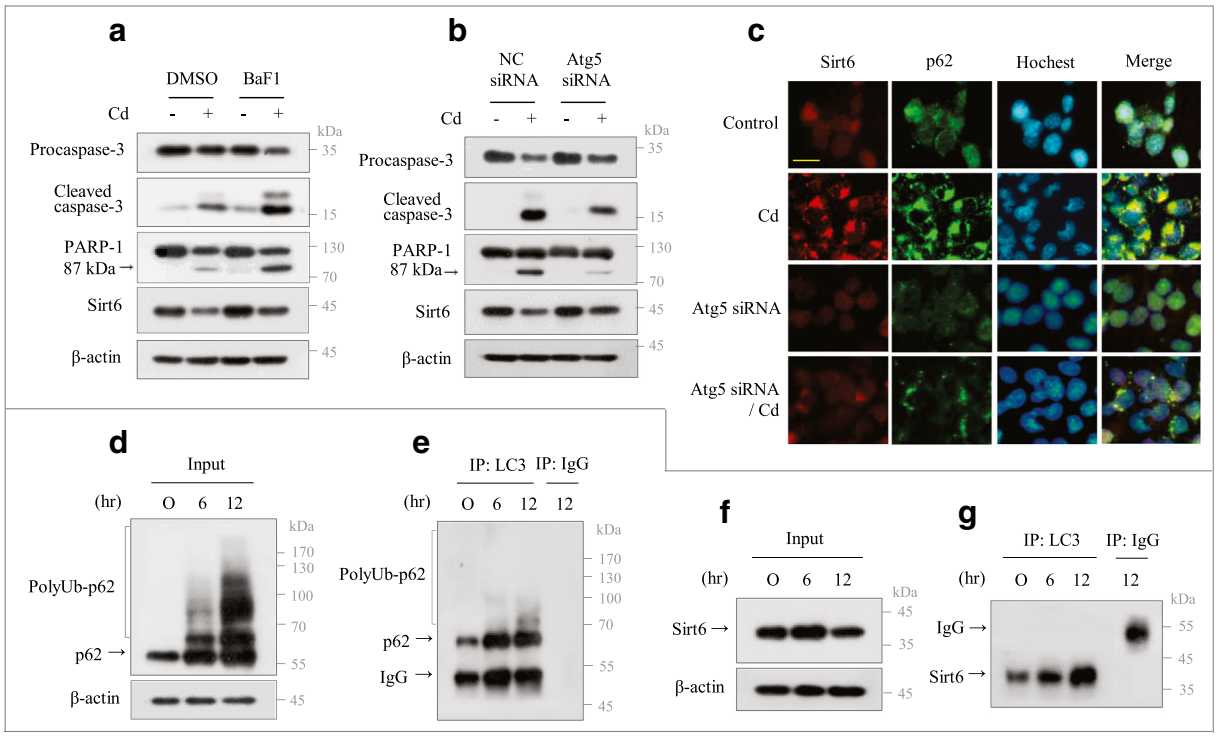

Fig. 7 Polyubiquitination of p62 targets Sirt6 to autophagosomes. **a** Cells were pretreated with 20 nM BaF1 for 2 h, and then exposed to 24 μM Cd for 12 h. Immunoblotting was performed for indicated proteins. **b** Cells transfected with NC and *Atg5*-specific siRNAs were treated with 24 μM Cd for 12 h. Immunoblotting was performed for indicated proteins. **c** Cells were transfected with Sirt6 siRNA and exposed to Cd for 12 h prior to fixation. Cells were incubated with p62 (green) and Sirt6 (red) antibodies. Nuclei were counterstained with Hoechst 33342. Scale bar, 25 μm. **d**–**g** Cells were treated with 24 μM Cd for 6 h and 12 h. **d**, **f** Immunoblotting was performed with p62 or Sirt6 antibodies. **e**, **g** Immunoprecipitation was performed with 600 μg of remaining protein with LC3B antibody or rabbit IgG, and then immunoblotting was performed with p62 or Sirt6 antibodies, respectively. β-actin was used as the loading control

The involvement of PolyUb-p62/Sirt6 signaling in Cd resistance and Cd toxicity in mouse kidney mesangial cells

We showed that polyUb-p62 caused Cd-induced apoptosis via Sirt6 accumulation in the cytoplasm. We next examined whether polyUb-p62/Sirt6 signaling was associated with Cd resistance. A Cd-resistant MES13 cell line (RMES13) was established after several rounds of selection by exposing MES13 cells to a stepwise series of increasing Cd concentrations. These cells showed 4-fold higher resistance to Cd than that by wild-type MES13 cells (data not shown). Cd-treated RMES13 cells showed complete inhibition of polyUb-p62 and autophagy, with no changes in Sirt6 levels compared with those in untreated control RMES13 cells. Consistent with these findings, Cd-treated RMES13 cells showed inhibited caspase-3-mediated PARP-1 cleavage, indicating that polyUb-p62 was involved in Cd-induced apoptosis through Sirt6 regulation (Fig. 8a).

Next, we examined whether polyUb-p62/Sirt6 signaling was involved in Cd-induced kidney toxicity in an in vivo model. Mice were exposed to Cd by intraperitoneal (i.p.) injection for 4 weeks, as previously described (Park et al. 2013) Glomerular mesangial cells were observed at 1 and 4 weeks after Cd injection, and protein extracts were prepared for immunoblotting. After 1 week, Cd treatment slightly induced autophagy but did not cause notable changes in other proteins. However, in mice treated with Cd for 4 weeks, significant increases in p62, LC3-II, Sirt6, and cleaved caspase-3 were observed compared with those in saline-injected control mice (Fig. 8b, c). Evaluation of morphological changes in kidney tissues using hematoxylin and eosin (H&E) staining after 4 weeks showed hypertrophied glomeruli and tubular epithelial cells in Cd-treated mice compared with saline-injected control mice (Fig. 8d-i,

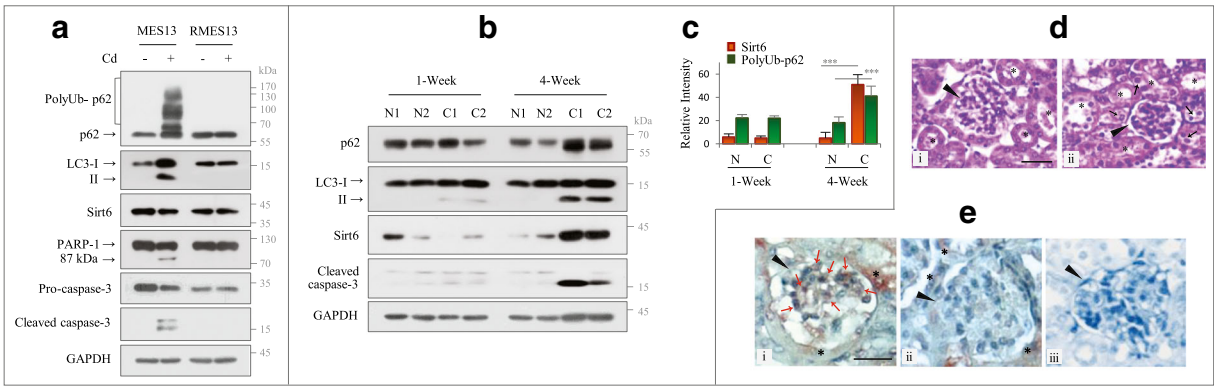

Fig. 8 Expressions of polyUb-p62 and Sirt6 in Cd-resistant cells (RMES13) and Cd-injected glomerular mesangial cells. **a** RMES13 cells constitutively expressed Sirt6 and suppressed polyubiquitination of p62. MES13 and RMES13 cells were exposed to 30 μM Cd for 12 h. Immunoblotting was performed for indicated proteins, where β-actin was used as the loading control. $n = 3$. **b**, **c** Mice were exposed to saline (N) or Cd (C) through i.p. injection for 4 weeks, and kidney tissue lysates were analyzed for indicated proteins by immunoblotting. GAPDH was used as the loading control. p62 levels were quantified by densitometry and normalized to GAPDH. Data are represented as mean ± SD ($n = 8$). $^{***}P < 0.0005$. **d** Histological changes (H&E staining) of kidney tissues after saline (i) and Cd (ii) injection in mice after 4 weeks. × 400. (i) Normal glomerulus (arrow head) and tubules (asterisks) from the medulla are shown. (ii) Hypertrophied glomeruli (arrow head) and tubular epithelial cells (arrows) are shown. Scale bar = 50 μm. **e** Immunohistochemical analysis of Sirt6 in kidney tissues of (i) Cd- and (ii) saline- injected mice. (iii) Negative control × 400. Red arrows and asterisks indicate Sirt6 in glomerular mesangial cells and tubular epithelial cells, respectively. Arrow heads, glomerulus. Scale bar = 50 μm

ii). Additionally, immunohistochemical (IHC) staining for Sirt6 revealed that Sirt6 immunoreactivity in Cd-treated mice was high in the cytosol of mesangial cells and tubular epithelial cells (Fig. 8e-i). In control kidney tissues, positive immunoreactivity for Sirt6 was not observed in glomerular mesangial cells, although some tubular epithelial cells showed positive Sirt6 staining (Fig. 8e-ii). The negative control (antibody dilution buffer instead of anti-Sirt6 antibodies) did not show positive immunoreactivity (Fig. 8e-iii). These data suggested that cytosolic localization of Sirt6 in mesangial cells could be a marker of Cd-induced glomerular damage.

Discussion

Sirt6 plays critical roles in maintaining kidney homeostasis and function (Huang et al. 2017). However, its involvement in heavy metal–induced kidney damage has not been elucidated. In this study, we demonstrated the role of Sirt6 in Cd toxicity and underlying molecular mechanisms in glomerular mesangial cells. We found that subcellular redistribution of Sirt6 played critical roles in Cd-induced apoptosis, which was regulated by polyUb-p62 and autophagy (Suppl. Fig. S9). The involvement of p62/Sirt6 signaling in Cd toxicity was confirmed in a Cd-resistant kidney cell line and Cd-injected mice. Thus, the p62/Sirt6 signaling pathway may be a promising target for managing kidney diseases. To our knowledge, this is the first study demonstrating the function of Sirt6 in heavy metal–induced apoptosis in the kidney through in vivo and in vitro experiments.

p62 is a multifunctional protein that contains various protein–protein interaction domains, including N-terminal Phox/Bem1p (PB1), a nuclear localization signal (NLS), a nuclear export signal (NES), an LC3-interacting region (LIR), and a C-terminal Ub-associated (UBA) domain. The most well-characterized function of p62 is a key role in intracellular quality control via selective autophagy, where p62 interacts with ubiquitinated cargo via the UBA domain and then recruits them into the autophagosomes through its interaction with the LIR domain. p62 also facilitates shuttling of substrates to the proteasome. Furthermore, p62 is involved in nuclear quality control by shuttling between the nucleus and cytoplasm via the NLS and NES (Liu et al. 2016; Moscat and Diaz-Meco 2009). In our study, despite induction of LC3-II after Cd exposure, p62 levels increased and were polyubiquitinated. However, another LC3-binding protein, NBR1, was downregulated, indicating that Cd-induced autophagy could interrupt p62-mediated selective autophagic degradation. In this study, we did not elucidate how p62-mediated autophagic degradation

was selectively and transiently impaired, and the underlying molecular mechanisms remain to be determined. Notably, p62 plays critical roles in the formation of ubiquitinated protein aggregates, which act as a signaling hub for cell death and survival (Moscat and Diaz-Meco 2009). We hypothesized that polyUb-p62 accumulation after Cd exposure may be associated with Cd-induced cytotoxicity in MES13 cells. We confirmed that p62 KD suppressed Cd-induced apoptosis. Moreover, we found that Cd resistance was associated with suppressing polyubiquitination of p62.

Mammalian sirtuins (Sirt1–7) are conserved NAD-dependent protein deacetylases. Sirt6 uniquely functions as both a deacetylase and a mono-ADP-ribosyltransferase ribosyltransferase (Liszt et al. 2005; Lombard et al. 2008). Sirt6 can deacetylate histone H3K9 and K56 residues and C-terminal binding protein interacting protein (CtIP) (Kaidi et al. 2010; Michishita et al. 2008). Different members of the sirtuin family are differentially localized and have different functions (Michishita et al. 2005; Santos et al. 2016). Thus, changes in subcellular localization and expression are associated with several types of diseases (Morigi et al. 2018; Wang et al. 2019). Subcellular localization and protein expression levels can be important factors related to nuclear functions of Sirt6. At the transcriptional level, Sirt6 is positively regulated by c-Fos, p53, and the Sirt1/FOX3a/NRF1 complex (Yuan et al. 2010). Additionally, stability of Sirt6 protein is regulated by the ubiquitin ligase C-terminus of Hsp70-interacting protein or the Sirt6-specific deubiquitinase USP10 (Lin et al. 2013; Ronnebaum et al. 2013), suggesting that Sirt6 may interact with Ub. Our results revealed that Sirt6 indirectly interacted with Ub via p62 (Fig. 6), where Sirt6 accumulated in the cytosol and was degraded. Subcellular fractionation analysis showed that Sirt6 was mostly present in the insoluble fraction, with small amounts in the particulate fractions, demonstrating that Sirt6 was primarily present as a membrane-bound protein or inside organelles. We then tested how nuclear Sirt6 translocated to components of the particulate fractions, and hypothesized that Sirt6 translocation may be dependent on p62, which has both an NLS and NES (Lin et al. 2013; Yuan et al. 2010). We confirmed that Sirt6 and p62 interact by IP and IF assays. p62 deficiency thus resulted in Sirt6 stabilization in the nucleus. Furthermore, treatment with LMB inhibited polyUb-p62 and Sirt6 accumulation in the particulate fractions, indicating that subcellular redistribution of Sirt6 depended on p62. Nuclear stabilization of Sirt6, due to p62 deficiency, decreased the number of cells with nuclear apoptotic changes, indicating that Sirt6 accumulation in the cytosol caused apoptosis. Many studies have shown that Sirt6 is critical in inducing apoptosis in cancer cells, including hepatocellular carcinoma cells, HeLa cells, endometrial cancer cells, and MDA-MB-231 cells. However, this is not the case in normal cells, such as WI38 lung epithelial cells and primary human mammary epithelial cell lines (HMEC1, HMEC2) (Fukuda et al. 2015; Van Meter et al. 2011; Zhang et al. 2009). Additionally, in mouse embryonic fibroblasts derived from Sirt6-knockout mice, apoptosis was induced by various stressors, including starvation. Sirt6-deficient cells resisted apoptosis by delaying initiation. However, once apoptosis was initiated, it progressed quicker than that in wild-type cells (Domanskyi et al. 2017). Therefore, inconsistent results in previous studies may be a result of differential Sirt6 subcellular localization. Sirt6 was downregulated during Cd treatment in MES13 cells. Cells overexpressing Sirt6 responded to Cd-induced apoptosis in a biphasic pattern that was dependent on Sirt6 subcellular localization. When Sirt6 nuclear expression was higher than cytoplasmic expression, Cd-induced apoptosis was inhibited, and vice versa, compared with that in wild-type cells (Suppl. Fig. S4b-d). Our current findings revealed that the interaction between p62 and Sirt6 was critical for Cd cytotoxicity. We confirmed that Cd-resistant MES13 cells inhibited polyubiquitination of p62. This resulted in constitutively expressed Sirt6 in response to Cd, thereby inhibiting autophagy and apoptosis. Consistently, mice exposed to Cd for over 4 weeks showed significant p62 and Sirt6 accumulation in kidney tissues compared with that in control mice, resulting in increased autophagy and apoptosis. Therefore, our in vitro and in vivo studies confirmed that p62/Sirt6 signaling could play a critical role in Cd-induced kidney damage.

In this study, Cd exposure induced Sirt6 translocation with p62 into the cytosol, resulting in transient aggregation. Therefore, we investigated how the Sirt6/p62 complex transiently avoided autophagic degradation. Since p62 is an autophagy adaptor protein, Sirt6 can be recruited to the autophagosome by p62. We observed that LC3B interacted with p62 and Sirt6, and that autophagy impairment via *Atg5* KD inhibited cytosolic translocation of Sirt6, thereby promoting nuclear accumulation. Furthermore, treatment with BaF1, a late-stage autophagy inhibitor, enhanced Cd-induced Sirt6 and polyUb-p62 aggregation in the cytosol. Therefore, transient accumulation of Sirt6 after Cd exposure could be caused by impaired autophagic degradation.

To date, most in vivo and in vitro studies have evaluated cellular disease mechanisms involved with Cd toxicity. These studies have focused on Cd-induced apoptotic cell death, which is caused by oxidative stress (Ravindran et al. 2016). Therefore, we tested whether polyubiquitination of p62 was associated with Cd-dependent reactive oxygen species (ROS) production. We found that treatment with *N*-acetyl cysteine completely suppressed Cd-induced polyubiquitination of p62 and upregulated Sirt6 expression (Suppl. Fig. S8). Thus, Cd-induced oxidative stress may be critical in regulating p62 polyubiquitination and subsequent Sirt6 translocation. However, further studies are required to confirm these results.

In conclusion, we demonstrated that p62-mediated Sirt6 translocation was critical in Cd toxicity in kidney cells and mouse kidneys, where nuclear Sirt6 was targeted by polyUb-p62 to the autophagosome. Therefore, Sirt6 may serve as a therapeutic target for treating kidney diseases. Furthermore, our results suggested that Cd resistance was associated with persistent Sirt6 expression by inhibiting polyubiquitination of p62, which may be critical for Cd-induced carcinogenesis.

Authors' contributions KYS and SHO designed the study and performed experiments. SHO and BHP performed animal study and generated the figures. SHO wrote the paper. All authors analyzed data, reviewed and edited the manuscript, and provided fundings.

Funding information This research was supported by Basic Science Research Program through the National Research Foundation of Korea (NRF) funded by the Ministry of Education (NRF-2013R1A1A2058384) and by grants from the Medical Research Center Program (NRF-2017R1A5A2015061) through the National Research Foundation (NRF), which is funded by the Korean government (MSIP) and grants from the Clinical Medcine Research Institute at Chosun University Hospital (2015).

Compliance with ethical standards All protocols for animal experiments were approved by the Institutional Animal Care and Use Committee (IACUC) at Chosun University (No.CIACUC2019-A0045).

Conflict of interest The authors declare that they have no competing interests.

References

Chargui A, Zekri S, Jacquillet G, Rubera I, Ilie M, Belaid A, et al. Cadmium-induced autophagy in rat kidney: an early biomarker of subtoxic exposure. Toxicol Sci. 2011;121:31–42.

Domanskyi S, Nicholatos JW, Schilling JE, Privman V, Libert S. SIRT6 knockout cells resist apoptosis initiation but not progression: a computational method to evaluate the progression of apoptosis. Apoptosis. 2017;22:1336–43.

Fan H, Yang HC, You L, Wang YY, He WJ, Hao CM. The histone deacetylase, SIRT1, contributes to the resistance of young mice to ischemia/reperfusion-induced acute kidney injury. Kidney Int. 2013;3:404–13.

Fujishiro H, Liu Y, Ahmadi B, Templeton DM. Protective effect of cadmium-induced autophagy in rat renal mesangial cells. Arch Toxicol. 2018;92:619–31.

Fujiwara Y, Lee JY, Tokumoto M, Sathh M. Cadmium renal toxicity via apoptotic pathways. Biol Pharm Bull. 2012;35:1892–7.

Fukuda T, Wada-Hiraike O, Oda K, Tanikawa M, Makii C, Inaba K, et al. Putative tumor suppression function of SIRT6 in endometrial cancer. FEBS Lett. 2015;589:2274–81.

Guyton AC. Blood pressure control–special role of the kidneys and body fluids. Science. 1991;252:1813–6.

Hasegawa K, Wakino S, Yoshioka K, Tatematsu S, Hara Y, Minakuchi H, et al. Kidney-specific overexpression of Sirt1 protects against acute kidney injury by retaining peroxisome function. J Biol Chem. 2010;285:13045–56.

He W, Wang Y, Zhang MZ, You L, Davis LS, Fan H, et al. Sirt1 activation protects the mouse renal medulla from oxidative injury. J Clin Invest. 2010;120:1056–68.

Huang W, Liu H, Zhu S, Woodson M, Liu R, Tilton RG, et al. Sirt6 deficiency results in progression of glomerular injury in the kidney. Aging (Albany NY). 2017;9:1069–83.

Ichimura Y, Kominami E, Tanaka K, Komatsu M. Selective turnover of p62/A170/SQSTM1 by autophagy. Autophagy. 2008;4:1063–6.

Järup L. Hazards of heavy metal contamination. Br Med Bull. 2003;68:167–82.

Johri N, Jacquillet G, Unwin R. Heavy metal poisoning: the effects of cadmium on the kidney. Biometals. 2010;23:783–92.

Kaidi A, Weinert BT, Choudhary C, Jackson SP. Human SIRT6 promotes DNA end resection through CtIP deacetylation. Science. 2010;329:1348–53.

Kim HR, Lee KY, Ahn SG, Lee BH, Jung KT, Yoon JH, et al. Transcriptional regulation, stabilization, and subcellular redistribution of multidrug resistance-associated protein 1 (MRP1) by glycogen synthase kinase 3αβ: novel insights on modes of cadmium-induced cell death stimulated by MRP1. Arch Toxicol. 2015;89:1271–84.

Kimura T, Isaka Y, Yoshimori T. Autophagy and kidney inflammation. Autophagy. 2017;13:997–1003.

Kroemer G, Mariño G, Levine B. Autophagy and the integrated stress response. Mol Cell. 2010;40:280–93.

Kirkin V, Lamark T, Sou YS, Bjørkøy G, Nunn JL, Bruun JA, et al. A role for NBR1 in autophagosomal degradation of ubiquitinated substrates. Mol Cell. 2009;33:505–16.

Kitada M, Kume S, Takeda-Watanabe A, Kanasaki K, Koya D. Sirtuins and renal diseases: relationship with aging and diabetic nephropathy. Clin Sci (Lond). 2013;124:153–64.

Kitamura M, Hiramatsu N. The oxidative stress: endoplasmic reticulum stress axis in cadmium toxicity. Biometals. 2010;23:941–50.

Lee SA, Cozzi M, Bush EL, Rabb H. Distant organ dysfunction in acute kidney injury: a review. Am J Kidney Dis. 2018;72:846–56.

Levine B, Yuan J. Autophagy in cell death: an innocent convict? J Clin Invest. 2005;115:2679–88.

Liang C, Jung JU. Autophagy genes as tumor suppressors. Curr Opin Cell Biol. 2010;22:226–33.

Lin Z, Yang H, Tan C, Li J, Liu Z, Quan Q, et al. USP10 antagonizes c-Myc transcriptional activation through SIRT6 stabilization to suppress tumor formation. Cell Rep. 2013;5: 1639–49.

Liszt G, Ford E, Kurtev M, Guarente L. Mouse Sir2 homolog SIRT6 is a nuclear ADP-ribosyltransferase. J Biol Chem. 2005;280:21313–20.

Liu M, Liang K, Zhen J, Zhou M, Wang X, Wang Z, et al. Sirt6 deficiency exacerbates podocyte injury and proteinuria through targeting Notch signaling. Nat Commun. 2017;8: 413–27.

Liu WJ, Ye L, Huang WF, Guo LJ, Xu ZG, Wu HL, et al. p62 links the autophagy pathway and the ubiqutin-proteasome system upon ubiquitinated protein degradation. Cell Mol Biol Lett. 2016;21:29–42.

Lombard DB, Schwer B, Alt FW, Mostoslavsky R. SIRT6 in DNA repair, metabolism and ageing. J Intern Med. 2008;263:128–41.

Luo B, Lin Y, Jiang S, Huang L, Yao H, Zhuang Q, et al. Endoplasmic reticulum stress eIF2α-ATF4 pathway-mediated cyclooxygenase-2 induction regulates cadmium-induced autophagy in kidney. Cell Death Dis. 2016;7:e2251.

Luo T, Yuan Y, Yu Q, Liu G, Long M, Zhang K, et al. PARP-1 overexpression contributes to cadmium-induced death in rat proximal tubular cells via parthanatos and the MAPK signalling pathway. Sci Rep. 2017;7:4331–43.

Michishita E, Park JY, Burneskis JM, Barrett JC, Horikawa I. Evolutionarily conserved and nonconserved cellular localizations and functions of human SIRT proteins. Mol Biol Cell. 2005;16:4623–35.

Michishita E, McCord RA, Berber E, Kioi M, Padilla-Nash H, Damian M, et al. SIRT6 is a histone H3 lysine 9 deacetylase that modulates telomeric chromatin. Nature. 2008;452:492–6.

Morigi M, Perico L, Benigni A. Sirtuins in renal health and disease. J Am Soc Nephrol. 2018;29:1799–809.

Moscat J, Diaz-Meco MT. p62 at the crossroads of autophagy, apoptosis, and cancer. Cell. 2009;137:1001–4.

Ouyang J, Zeng Z, Fang H, Li F, Zhang X, Tan W. SIRT3 inactivation promotes acute kidney injury through elevated acetylation of SOD2 and p53. J Surg Res. 2019;233:221–30.

Pankiv S, Lamark T, Bruun JA, Øvervatn A, Bjørkøy G, Johansen T. Nucleocytoplasmic shuttling of p62/SQSTM1 and its role in recruitment of nuclear polyubiquitinated proteins to promyelocytic leukemia bodies. J Biol Chem. 2010;285: 5941–53.

Park CH, Lee BH, Ahn SG, Yoon JH, Oh SH. Serine 9 and tyrosine 216 phosphorylation of GSK-3β differentially regulates autophagy in acquired cadmium resistance. Toxicol Sci. 2013;135:380–9.

Ravindran G, Chakrabarty D, Sarkar A. Cell specific stress responses of cadmium-induced cytotoxicity. Anim Cells Syst (Seoul). 2016;21:23–30.

Ronnebaum SM, Wu Y, McDonough H, Patterson C. The ubiquitin ligase CHIP prevents SirT6 degradation through noncanonical ubiquitination. Mol Cell Biol. 2013;33:4461–72.

Santos L, Escande C, Denicola A. Potential modulation of sirtuins by oxidative stress. Oxidative Med Cell Longev. 2016;2016: 1–12.

Satarug S, Moore MR. Adverse health effects of chronic exposure to low-level cadmium in foodstuffs and cigarette smoke. Environ Health Perspect. 2004;112:1099–103.

So KY, Oh SH. Cadmium-induced heme-oxygenase-1 expression plays dual roles in autophagy and apoptosis and is regulated by both PKC-δ and PKB/Akt activation in NRK52E kidney cells. Toxicology. 2016;370:49–59.

Trzcinka-Ochocka W, Jakubowski M, Razniewska G, Halatek T, Gazewski A. The effects of environmental cadmium exposure on kidney function: the possible influence of age. Environ Res. 2004;95:143–50.

Van Meter M, Mao Z, Gorbunova V, Seluanov A. SIRT6 overexpression induces massive apoptosis in cancer cells but not in normal cells. Cell Cycle. 2011;10:3153–8.

Wang SH, Shih YL, Kuo TC, Ko WC, Shih CM. Cadmium toxicity toward autophagy through ROS-activated GSK-3beta in mesangial cells. Toxicol Sci. 2009;108:124–31.

Wang Y, He J, Liao M, Hu M, Li W, Ouyang H, et al. An overview of sirtuins as potential therapeutic target: structure, function and modulators. Eur J Med Chem. 2019;161:48–77.

Wu H, Liao Q, Chillrud SN, Yang Q, Huang L, Bi J, et al. Environmental exposure to cadmium: health risk assessment and its associations with hypertension and impaired kidney function. Sci Rep. 2016;6:1–9.

Yu W, Dittenhafer-Reed KE, Denu JM. SIRT3 protein deacetylates isocitrate dehydrogenase 2 (IDH2) and regulates mitochondrial redox status. J Biol Chem. 2012;287:14078–86.

Yuan J, Luo K, Zhang L, Cheville JC, Lou Z. USP10 regulates p53 localization and stability by deubiquitinating p53. Cell. 2010;140:384–96.

Zhang D, Li S, Cruz P, Kone BC. Sirtuin 1 functionally and physically interacts with disruptor of telomeric silencing-1 to regulate alpha-ENaC transcription in collecting duct. J Biol Chem. 2009;284:20917–26.